Inorganic Chemistry

Article

pubs.acs.org/IC

Synthesis, Crystal Structure, and TEM Analysis of $Sr_{19}Li_{44}$ and Sr_3Li_2: A Reinvestigation of the Sr−Li Phase Diagram

Volodymyr Smetana,*[,†,‡] Lorenz Kienle,[†,§] Viola Duppel,[†] and Arndt Simon[†]

[†]Max-Planck-Institut für Festkörperforschung, Heisenbergstrasse 1, D-70569 Stuttgart, Germany

[‡]Ames Laboratory−DOE, Iowa State University, Ames, Iowa 50011, United States

[§]Institut für Materialwissenschaft, Kaiserstrasse 2, D-24143 Kiel, Germany

Supporting Information

ABSTRACT: Two intermetallic phases in the Sr−Li system have been synthesized and structurally characterized. According to single-crystal X-ray diffraction data, $Sr_{19}Li_{44}$ and Sr_3Li_2 crystallize with tetragonal unit cells ($Sr_{19}Li_{44}$, *I*-42*d*, a = 15.9122(7) Å, c = 31.831(2) Å, Z = 4, V = 8059(2) Å^3; Sr_3Li_2, $P4_2/mnm$, a = 9.803(1) Å, c = 8.784(2) Å, Z = 4, V = 844.2(2) Å^3). The first compound is isostructural with the recently discovered $Ba_{19}Li_{44}$. Sr in $Sr_{19}Li_{44}$ can be fully replaced by Ba with no changes to the crystal structure, whereas the substitution of Sr by Ca is only possible within a limited concentration range. Sr_3Li_2 can be assigned to the Al_2Zr_3 structure type. The crystal structure determination of $Sr_{19}Li_{44}$ was complicated by multiple twinning. As an experimental highlight, an electron microscopy investigation of the highly moisture- *and* electron-beam-sensitive crystals was performed, enabling high-resolution imaging of the defect structure.

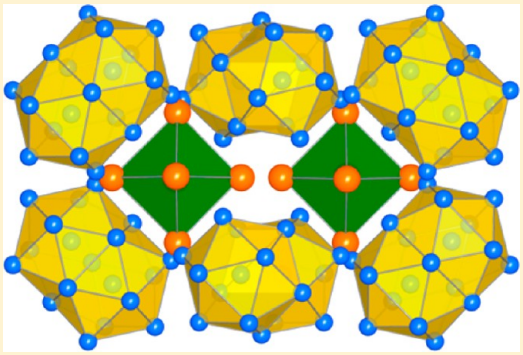

INTRODUCTION

The chemistry of intermetallic compounds of alkali and alkaline-earth metals has been considerably developed within the last 20 years. All binary compounds in these systems are restricted to light alkali-metal representatives containing Li and Na. Two compounds are known in the system Na−Ba (Na_2Ba[1] and NaBa),[2] one with Ca and Li, represented by the two modifications of $CaLi_2$,[3,4] two with Sr and Li (Sr_6Li_{23}[5] and Sr_3Li_2),[6] and one with Ba and Li, namely, $BaLi_4$.[7,8] In the course of our investigations, $Ba_{19}Li_{44}$[9] was found as a second representative. Because Ba and Sr have very similar atomic radii, we decided to investigate more accurately the Sr−Li system in order to check the existence of $Sr_{19}Li_{44}$ or other chemically or structurally related phases. It is worth noting that Sr_3Li_2 was reported to exhibit short Li−Li distances (approximately 2.2 Å), which might indicate contamination by some electronegative element, e.g., N. $Li_{80}Ba_{39}N_9$[10] exhibits very similar Li−Li contact lengths; however, no such compound is known in the systems Sr−Li−N(O,H).

A number of ternary compounds with very complicated structures was observed in the systems Li−Ba−Ca and Li−Na−Ba. $Li_{13}Na_{29}Ba_{19}$[11] represents a complex variant of the rock-salt-type structure with a novel Li_{26} anti-Mackay cluster. $Li_{33.3}Ba_{13.1}Ca_3$ and similar $Li_{18.9}Na_{8.3}Ba_{15.3}$[12] are characterized by giant unit cells, clearly highlighting their structural complexity within the family of intermetallic compounds. They exhibit next members of the Li anti-Mackay family, Li_{19}, and stabilizing roles of a third element in the structure formation. $Li_{33.3}Ba_{13.1}Ca_3$ crystallizes in a rhombohedral cell, while $Li_{18.9}Na_{8.3}Ba_{15.3}$ in a primitive one, however with very close lattice parameters. In order to clarify their structures, the Li−Na−Ba system was investigated with transmission electron microscopy (TEM). This work was very helpful in explaining some problematic structure details mainly caused by crystal twinning. Thus, TEM on the moisture- and beam-sensitive samples appears to be the suitable tool for solving similar problems in the Sr−Li system.

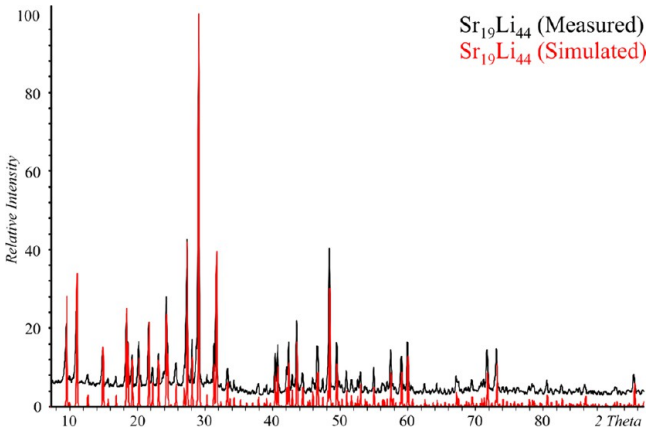

Figure 1. Measured and simulated XRD patterns of $Sr_{19}Li_{44}$.

Special Issue: To Honor the Memory of Prof. John D. Corbett

Received: May 5, 2014
Published: June 27, 2014

EXPERIMENTAL SECTION

Synthesis. Single crystals of both compounds were obtained from the starting materials Sr metal (Merck, 99.9%; distilled twice with intermediate heating in a closed Ta container at 1200 K in vacuo to remove hydrogen) and Li metal (Merck, 99.5%). Both samples $Sr_{19}Li_{44}$ [Sr (500.0 mg) and Li (91.7 mg)] and Sr_3Li_2 [Sr (500 mg) and Li (26.6 mg)] were enclosed in Ta ampules in an Ar atmosphere. The reaction mixtures were heated to 280 °C at a rate of 50 °C·h^{-1} and kept at this temperature for 4 days. Then they were cooled to 120 °C at 1 °C·h^{-1} and annealed at this temperature for 3 weeks. $Sr_{19}Li_{44}$ was obtained pure according to powder X-ray diffraction (XRD) analysis (Figure 1); however, Sr_3Li_2 contained traces of $Sr_{19}Li_{44}$ and Sr. Both compounds are sensitive to air or moisture at room temperature.

XRD Studies. Single-crystal XRD data were collected at room temperature using a STOE IPDS II diffractometer with Mo Kα radiation by oscillation of the crystal around the ω axis. The starting atomic parameters derived via direct methods using the program *SIR 97*[13] were subsequently refined in the space group $I\bar{4}2d$ with use of the program *SHELX-97*[14] (full-matrix least squares on F^2) with anisotropic atomic displacement parameters for Sr atoms within the *WinGX* program package.[15] The positions of the Li atoms were found in difference Fourier maps according to reasonable interatomic distances between detected and new proposed atoms. Sr atoms were refined with anisotropic displacement parameters. The crystallographic files in CIF format for $Sr_{19}Li_{44}$, mixed $(BaSr)_{19}Li_{44}$, and Sr_3Li_2 have been deposited with FIZ Karlsruhe as CSD 421227, 421228, and 421229, respectively. The data may be obtained by contacting FIZ Karlsruhe at +497247808666 (fax) or via e-mail (crysdata@fiz-karlsruhe.de).

Electron Microscopy. High-resolution TEM (HRTEM), selected-area electron diffraction (SAED), and precession electron diffraction (PED) were performed with a CM 30ST electron microscope (Philips, LaB_6 cathode, accelerating voltage 300 kV), equipped with an energy-dispersive X-ray (EDX) system (Noran Co., Vantage System). The image was recorded with a multiscan CCD camera (Gatan). All manipulations for the preparation and transfer of the samples were carried out under dry Ar with the aid of a special device.[16,17] EDX analysis confirmed the functionality of the equipment because only marginal O Kα intensities

Table 1. Details of the Crystal Structure Investigation and Refinement for $Sr_{19}Li_{44}$

empirical formula	$Sr_{19}Li_{44}$
fw	1970.15
temperature, K	293(2)
wavelength, Å	0.560 86
cryst syst	tetragonal
space group	$I\bar{4}2d$
a, Å	15.9122(7)
c, Å	31.831(2)
volume, Å^3	8059(2)
Z	4
density (calcd), g·cm^{-3}	1.624
μ, mm^{-1}	12.45
cryst size, mm	0.14 × 0.10 × 0.12
$F(000)$	3415
θ range, deg	2.3−31.2
index ranges	$-23 \le h, k \le 23, -46 \le l \le 46$
reflns collected	47846
indep reflns	6578
refinement method	full-matrix least squares on F^2
data/restraints/param	6578/0/88
data averaging	R_{int} = 0.153, R_σ = 0.086
GOF on F^2	0.94
final R indices [$I > 2\sigma(I)$]	R1 = 0.051, wR2 = 0.085
R indices (all data)	R1 = 0.113, wR2 = 0.105
largest diff peak and hole, e·Å^{-3}	0.84 and −0.54

Table 2. Atomic Coordinates and Isotropic/Equivalent Thermal Displacement Parameters for $Sr_{19}Li_{44}$

atom	site	x	y	z	$U_{eq/iso}$
Sr1	4b	0.5	0.5	0	0.0288(3)
Sr2	8c	0.5	0	−0.15507(3)	0.0292(2)
Sr3	16e	0.58591(5)	0.09830(5)	0.04973(2)	0.0284(2)
Sr4	16e	0.40504(5)	0.10960(5)	−0.04698(2)	0.0292(2)
Sr5	16e	0.50457(6)	0.18934(4)	−0.24950(3)	0.0293(2)
Sr6	16e	0.64422(5)	0.34739(5)	0.07579(2)	0.0289(2)
Li1	16e	0.8181(8)	0.1736(8)	0.0871(3)	0.020(2)
Li2	16e	0.324(1)	−0.154(1)	−0.1614(5)	0.044(4)
Li3	8d	0.4575(15)	0.25	0.125	0.042(5)
Li4	16e	0.764(1)	0.513(1)	0.1314(5)	0.046(4)
Li5	16e	0.362(1)	−0.112(1)	−0.0682(5)	0.042(4)
Li6	16e	0.343(1)	0.133(1)	0.0660(5)	0.044(4)
Li7	16e	0.426(1)	0.065(1)	0.1429(4)	0.040(3)
Li8	16e	0.422(1)	0.292(1)	0.0337(5)	0.041(4)
Li9	16e	0.314(1)	−0.284(1)	−0.0951(5)	0.040(4)
Li10	16e	0.257(1)	−0.228(1)	−0.2430(5)	0.045(4)
Li11	8d	0.25	0.013(2)	−0.125	0.054(6)
Li12	16e	0.436(1)	−0.281(1)	−0.0317(6)	0.051(4)

Table 3. Anisotropic Thermal Displacement Parameters for $Sr_{19}Li_{44}$

atom	U_{11}	U_{22}	U_{33}	U_{23}	U_{13}	U_{12}
Sr1	0.0284(4)	0.0284(4)	0.0294(6)	0	0	0
Sr2	0.0328(5)	0.0288(5)	0.0261(4)	0	0	−0.0022(5)
Sr3	0.0299(4)	0.0265(4)	0.0286(3)	−0.0017(3)	−0.0011(3)	−0.0017(3)
Sr4	0.0313(4)	0.0285(4)	0.0278(4)	−0.0004(3)	0.0015(3)	−0.0009(3)
Sr5	0.0299(3)	0.0272(3)	0.0309(3)	−0.0001(3)	−0.0012(3)	−0.0007(4)
Sr6	0.0303(4)	0.0278(4)	0.0287(3)	0.0007(3)	0.0023(3)	−0.0015(3)

dx.doi.org/10.1021/ic5010165 | *Inorg. Chem.* 2015, 54, 733−739

occurred, so that hydrolysis of the sample could be minimized. The low melting temperatures of the investigated compounds led to the rapid decomposition of the sample in the electron beam. Because of that, TEM was possible only with an optimized beam diameter (spot 5–6) and relatively short exposure time (up to 1 s in the case of high-resolution images). A perforated C/Cu net served as the support for the crystallites. Using PED (applying "spinning star" by Nano-MEGAS; precession angle 3°), the multiple scattering could be reduced to a minimum.[18−22] Simulations of HRTEM images (multislice formalism[23,24]) and SAED patterns (kinematical approximation) were calculated with the *EMS* program package[25] (spread of defocus 70 Å; illumination semiangle 1.2 mrad). The software *Emaps* was used to simulate the PED patterns.[26] All images were recorded with a Gatan multiscan CCD camera and evaluated (including Fourier filtering) with the program *Digital Micrograph 3.6.1* (Gatan). All HRTEM images were filtered after Fourier transformation using a suitable band-pass mask.

RESULTS AND DISCUSSION

Crystal Structures. In this paper, we report on the new binary compound $Sr_{19}Li_{44}$ and a partial reinvestigation of the Sr−Li binary system. The compounds $Sr_{19}Li_{44}$ and Sr_3Li_2 crystallize in the tetragonal system with space groups $I\bar{4}2d$ and $P4_2/mnm$, respectively. Details of the data collection and structure refinement are listed in Tables 1 and 4. Anisotropic displacement parameters as well as atomic coordinates are given in Tables 2 and 3 and 5 and 6, respectively. According to the previous investigations, four compounds have been reported to exist in the Sr−Li binary system. In our work, the existence of Sr_3Li_2 and Sr_6Li_{23} has been confirmed, and a new compound that separates these phases according to an updated phase diagram Sr−Li has been discovered. We could not detect any traces of Sr_8Li or Sr_7Li mentioned in the previous work.[5] Samples with these compositions contain a mixture of Sr_3Li_2 and Sr. The updated phase diagram of the Sr−Li system is shown in Figure 2. $Sr_{19}Li_{44}$ undergoes a peritectoidal decomposition to Sr_3Li_2 and Sr_6Li_{23} at 148 °C, according to differential thermoanalysis (DTA) and temperature-dependent Guinier measurements, only 4 °C lower than the decomposition temperature of Sr_6Li_{23}. Sr_3Li_2 melts incongruently at 198 °C.

Sr_3Li_2 crystallizes in the Al_2Zr_3-type structure;[27] thus, it can be described as a packing of two different types of Sr_2Li_4

Table 4. Details of the Crystal Structure Investigation and Refinement for Sr_3Li_2

empirical formula	Sr_3Li_2
fw	276.74
temperature, K	293(2)
wavelength, Å	0.560 86
cryst syst	tetragonal
space group	$P4_2/mnm$
a, Å	9.803(1)
c, Å	8.784(2)
volume, Å^3	844.2(2)
Z	4
density (calcd), g·cm^{-3}	2.177
μ, mm^{-1}	18.77
cryst size, mm	0.13 × 0.11 × 0.12
F(000)	480
θ range, deg	3.11−26.36
index ranges	$-12 \le h, k \le 12, -10 \le l \le 10$
reflns collected	7512
indep reflns	503
refinement method	full-matrix least squares on F^2
data/restraints/param	354/0/14
data averaging	R_{int} = 0.143, R_σ = 0.048
GOF on F^2	1.02
final R indices [$I > 2\sigma(I)$]	R1 = 0.038, wR2 = 0.074
R indices (all data)	R1 = 0.065, wR2 = 0.080
largest diff peak and hole, e·Å^{-3}	1.01 and −0.52

Table 5. Atomic Coordinates and Isotropic/Equivalent Thermal Displacement Parameters for Sr_3Li_2

atom	site	x	y	z	$U_{eq/iso}$
Sr1	4f	0.1502(1)	0.1502(1)	0	0.0275(3)
Sr2	4g	0.2891(1)	−0.2891(1)	0	0.0302(3)
Sr3	4d	$^1/_2$	0	$^1/_4$	0.0272(3)
Li1	8j	0.388(2)	0.388(2)	0.182(2)	0.049(5)

Table 6. Anisotropic Thermal Displacement Parameters for Sr_3Li_2

atom	U_{11}	U_{22}	U_{33}	U_{23}	U_{13}	U_{12}
Sr1	0.0287(4)	U_{11}	0.0250(6)	0	0	0.0012(6)
Sr2	0.0321(5)	U_{11}	0.0264(7)	0	0	−0.0025(6)
Sr3	0.0278(4)	U_{11}	0.0260(6)	0	0	0

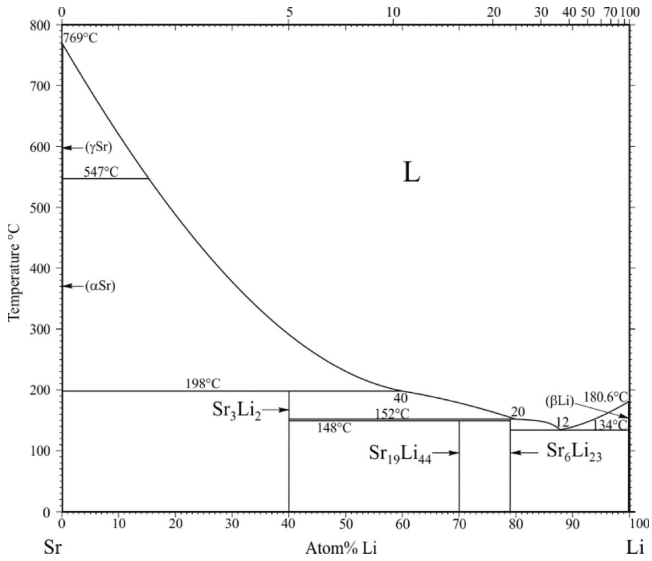

Figure 2. Equilibrium phase diagram of the Sr−Li system[5,6] complemented with the new compound $Sr_{19}Li_{44}$.

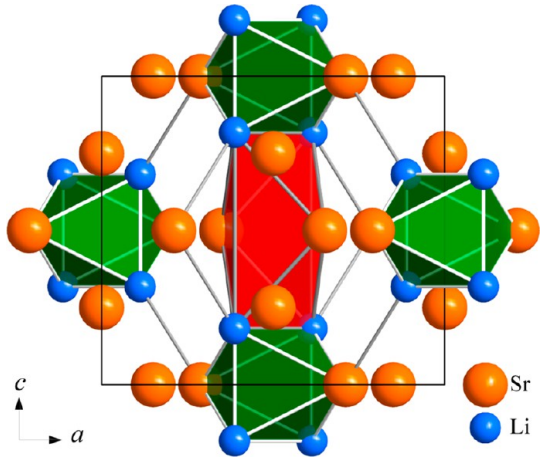

Figure 3. Crystal structure of Sr_3Li_2 viewed along the b axis.

dx.doi.org/10.1021/ic5010165 | Inorg. Chem. 2015, 54, 733−739

octahedra (elongated and squashed) with additional Sr atoms, forming bonds between them (Figure 3). Two Sr atoms exhibit a 14-fold coordination, and one has 15 near neighbors. Li atoms are 10-fold-coordinated building trigonal prisms capped by two Sr and two Li atoms. Within the Li substructure, the Li atoms form squares surrounded by only Sr atoms, forming larger $Sr_{20}Li_4$ clusters. In good agreement with the sum of metallic radii and in contrast to the values reported previously,[6] the Li−Li distances are in the range of 3.12(4)−3.20(4) Å and the Sr−Sr and Sr−Li contacts are in the ranges of 4.1388(5)−4.472(1) and 3.68(1)−4.00(1) Å, respectively.

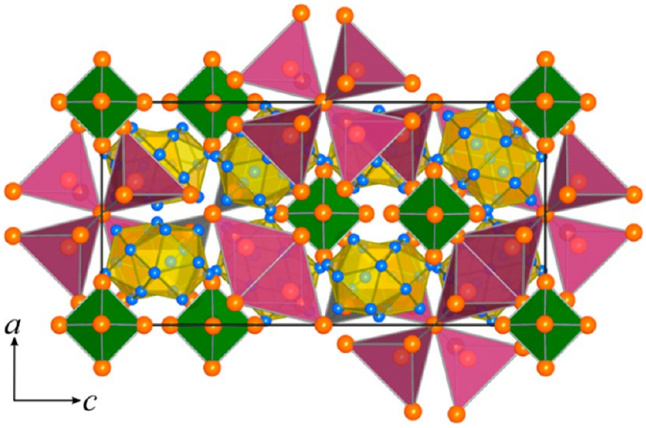

Figure 4. Ba_6 octahedra (green), quadruples of vertices sharing centered ($Ba_4Ba_{1/4}$) tetrahedra (violet), and Li_{19} anti-Mackay clusters (yellow) in the crystal structure of $Sr_{19}Li_{44}$. Sr atoms are marked in orange and Li atoms in blue.

$Sr_{19}Li_{44}$ belongs to the $Ba_{19}Li_{44}$ structure type. The crystal structure has been described in detail previously,[9] so only general comments and a comparison with the known phases will be provided. The basic structural units are empty Ba_6 octahedra, centered Ba_4 tetrahedra, and centered Li_{19} icosahedral clusters. Ba_6 and Ba_4 fragments establish a cubic-close-packed topology, and Li_{19} clusters fill tetrahedral voids corresponding to the chalcopyrite structure type (Figure 4). The Li−Li, Sr−Li, and Sr−Sr distances were found in the ranges of 2.94(3)−3.35(3), 3.71(1)−4.06(1), and 4.143(1)−4.234(1) Å, respectively, closely corresponding to the metal atom distances in $Ba_{19}Li_{44}$. Some short Li−Li distances between the central atoms of Li_{19}

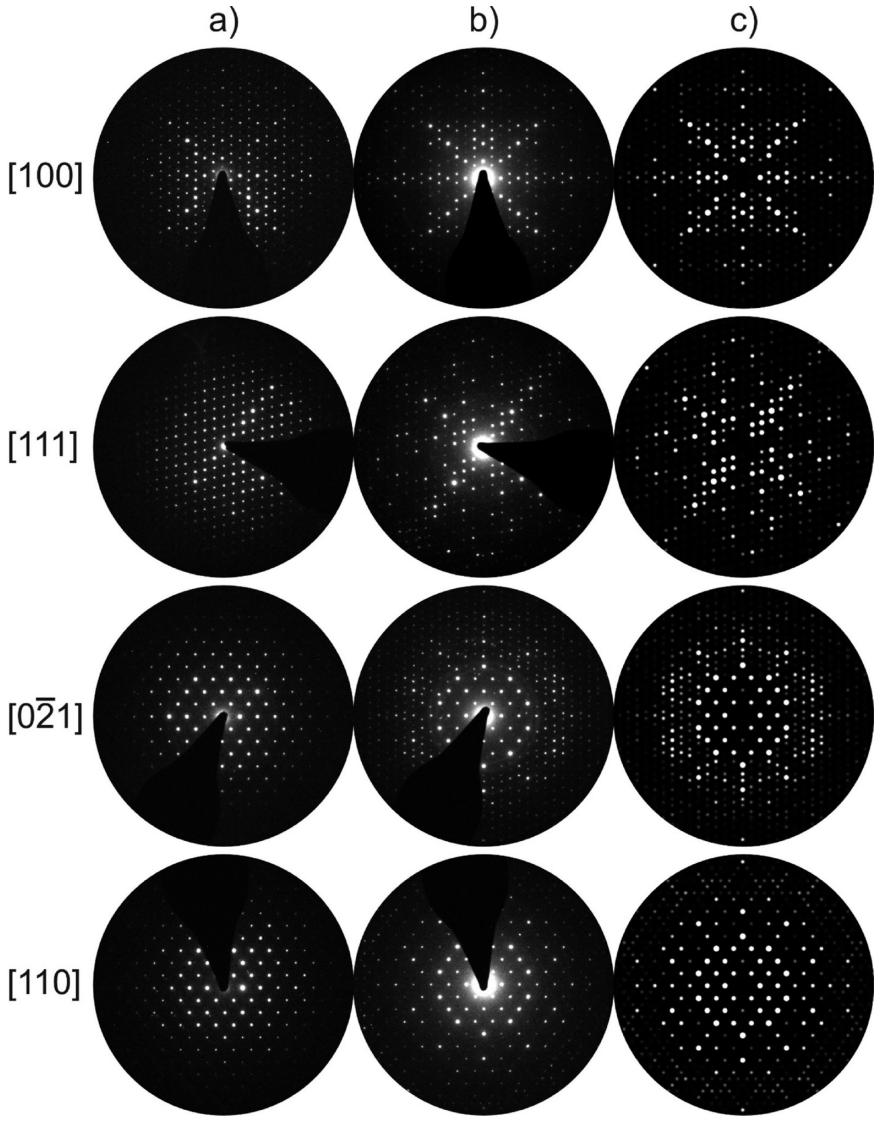

Figure 5. Experimental SAED (a) and PED (b) patterns with simulated PED patterns (c; precession angle 3°, thickness 15 nm). Zone axes are specified in the figure.

dx.doi.org/10.1021/ic5010165 | *Inorg. Chem.* 2015, 54, 733−739

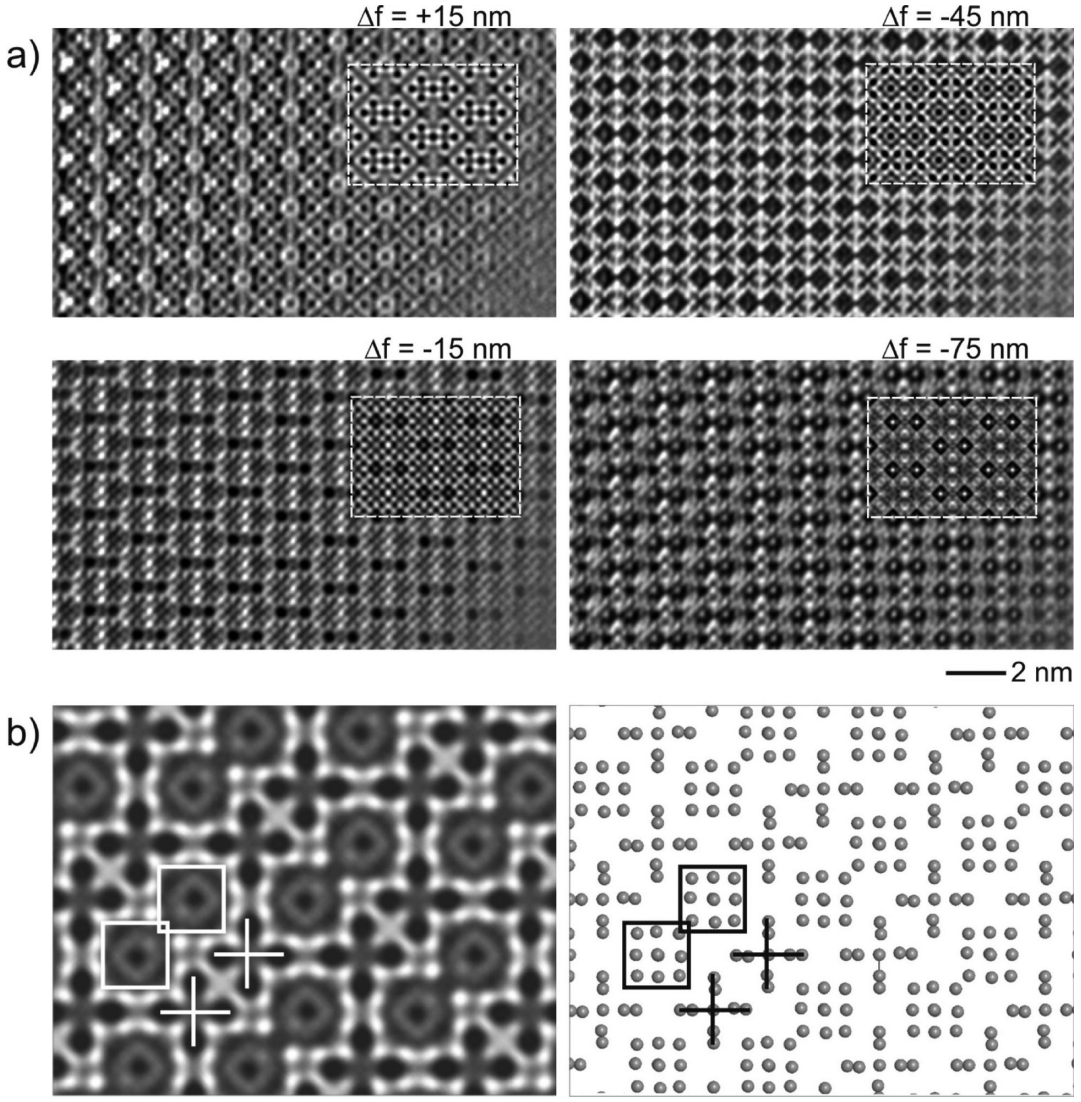

Figure 6. (a) HRTEM micrographs with inserted simulations based on the $Sr_{19}Li_{44}$-type structure (zone axis [100]; thickness 6.4 nm; focus values specified). (b) Interpretation of the Scherzer focus (simulated micrograph, left) by a projection of the Sr substructure (right).

clusters [2.78(3) and 2.81(2) Å] could be explained by the low accuracy of the Li coordinate determination due to the crystal quality or twinning. It should be noted that $Sr_{19}Li_{44}$ is the third representative of this structure type besides $Ba_{19}Li_{44}$ and the mixed phase $(Ba/Ca)_{19}(Ca/Li)_{44}$. A similar solid solution was also observed for mixed alkaline-earth-metal compounds containing Ba/Sr or Sr/Ca. It is known that Ca in such compounds can replace both the alkaline earth and Li.[12] However, Sr in the mixed phase was found only on joined sites with Ba. This observation can easily be explained by the geometrical factor: the difference between Li and Sr metallic radii is too large (1.56 vs 2.15 Å) to allow a common occupation of one position. From the electronic point of view, Li in these compounds can be considered as a formal anion, which, however, can play double roles and be present in both the cationic and anionic parts of the structure.[28,29] It should be emphasized that very similar to $Ba_{19}Li_{44}$, metal-rich nitride $Li_{80}Ba_{39}N_9$ is also known; however, all attempts to identify this compound with Sr failed. Trials to prepare $Li_{80}Sr_{39}N_9$ resulted in mixtures of $Sr_{19}Li_{44}$ and Sr_2N.[30] The isostructural compounds $Ba_{19}Li_{44}$ and $Sr_{19}Li_{44}$ show different thermal stability. Ba or mixed Ba/Ca phases decompose at approximately 125 °C and could be obtained only as a main component together with metallic Ba and $BaLi_4$-type phases. The sample prepared with the stoichiometric composition $Sr_{19}Li_{44}$ was observed as practically pure with negligible traces of Sr_3Li_2 and showed higher decomposition temperature, 148 °C.

HRTEM. The special metrics of $Sr_{19}Li_{44}$ ($c/a \sim 2$) indicate closeness to the cubic system. The cubic pseudosymmetry is expected to be indirectly preserved by the orientation of the triplet domains with the tetragonal structure as probable aspect of the real structure.[31] Indeed, XRD experiments on single crystals suggest the presence of twinning. The XRD patterns split into two sets of reflections; however, only one of them can be indexed assuming tetragonal metrics. The whole pattern indicates multiples of the unit cell parameters and (too high) cubic symmetry. These features are well-known for crystals twinned by partial merohedry; cf. the description of the triplets observed for tetragonal $CuGa_3Se_5$ with $c/a \sim 2$.[32]

Because of the ability of SAED to transmit small circular areas of the sample with 250 nm diameter, the structure of the single domains can be analyzed sequentially without superposition phenomena in reciprocal space. The above theory is demonstrated by the series of SAED, PED, and simulated PED

dx.doi.org/10.1021/ic5010165 | Inorg. Chem. 2015, 54, 733−739

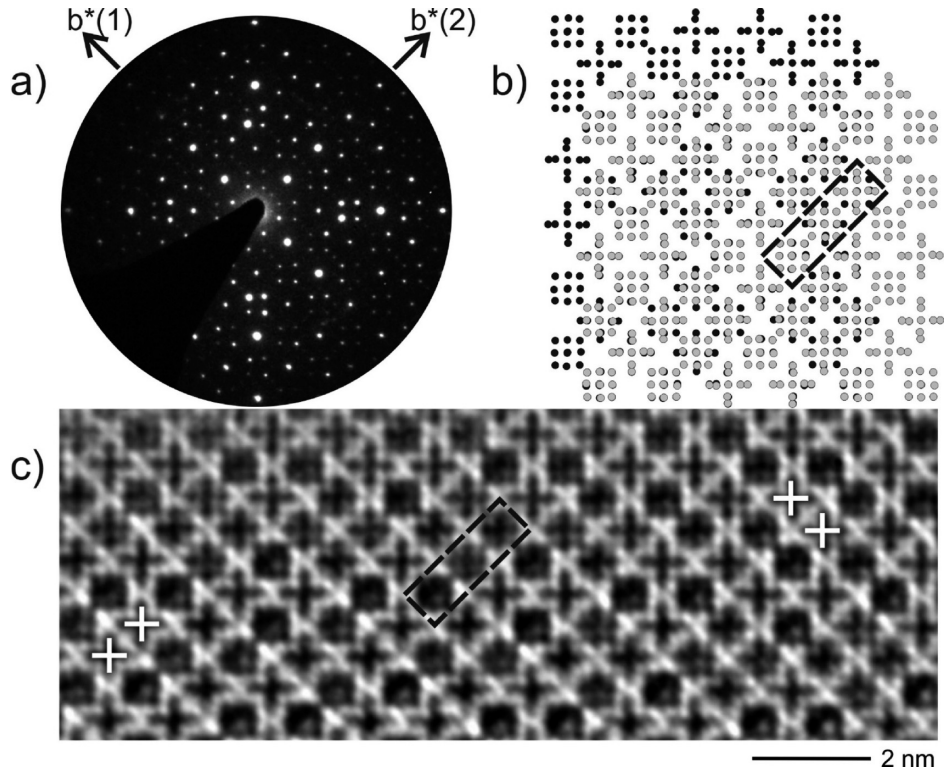

Figure 7. (a) SAED superposition pattern of domains of $Sr_{19}Li_{44}$ rotated by 90° in the plane of drawing. (b) Scheme of the Sr substructure displaying the superposition of twinned domains. (c) HRTEM micrograph recorded on twinned domains. Common zone axis [100] with marks for the structural interpretation; see the text.

patterns based on the tetragonal structure of $Sr_{19}Li_{44}$; cf. Figure 5. Note the advanced capabilities of the PED technique compared to the fixed-beam SAED, particularly with respect to the higher resolution (significant intensity for higher space frequencies) and weaker contribution from dynamical scattering. Moreover, intensities from higher-order Laue zones are only seen in the PED patterns; cf. the PED pattern along [0−21] containing a superposition of intensities from distinct Laue zones at high resolution. The particular advantages of PED versus conventional electron diffraction techniques become essential in the present case of a strongly moisture-sensitive sample. The thin areas at the crystal edges are frequently destroyed in the course of amorphization by hydrolysis. Thus, thicker sections of the crystallites must be analyzed where dynamical effects are intrinsically significant. Nevertheless, high-quality patterns close to the kinematic approximation can be recorded with the aid of PED, as demonstrated by the convincing agreement between the experimental and simulated PED patterns in Figure 5. Such a correlation strongly supports the assignment of $Sr_{19}Li_{44}$ to the tetragonal structure model.

Further evidence comes from HRTEM; cf. Figure 6a for images recorded with variable focus along the zone axis [100]. As verified by contrast simulation, for $\Delta f = -45$ nm, the imaging conditions of the Scherzer focus are approximated. Thus, assuming the weak-phase object approximation, the dark and bright spots in HRTEM micrographs represent high and low values of the projected potential, respectively. For the present case, the dark spots represent columns of the heavy Sr atoms; cf. the Sr substructure and simulated micrograph of Figure 6b. Along [100], the arrangement of the Sr atoms in quadruples of tetrahedra and the octahedral clusters is imaged by dark spots forming crosses and rounded squares, respectively (cf. marks in Figures 6b). Again the good correlation between the experimental images and simulated micrographs (see insets) proves $Sr_{19}Li_{44}$ and $Ba_{19}Li_{44}$ to be isostructural even for strongly underfocused images.

The twinning can be analyzed in real and reciprocal spaces; cf. Figure 7. The SAED pattern of Figure 7a was recorded inside a selected area containing a twin boundary with contributions of both domains. The patterns of the single domains on different sides of the twin boundary (not shown) are orthogonally oriented and match those expected for $Sr_{19}Li_{44}$. The superposition pattern represents the sum of both patterns with approximately 4-fold symmetry. The real structure at the twin interface is depicted by the HRTEM micrograph of Figure 7c. The image was recorded close to the Scherzer focus. The twinning is evident by the systematic arrangement of the characteristic contrasts representing the Sr substructure; i.e., the crosses and rounded squares already described for Figure 6a top, right. The orthogonal orientation of the pairs of crosses is obvious in the HRTEM micrograph, cf. marks in Figure 7c. However, at the interface, the superposition of the domains along the zone axis produces average contrast by the superposition of crosses and rounded squares. This inhibits a clear identification of the Sr cluster types at the twin interface. However, the average contrasts (e.g., rectangular mark in Figure 7c) evidence a variation in the cluster sequence for the twinned structure compared to the single domain structure.

■ CONCLUSIONS

Reinvestigation of the Sr−Li system resulted in the discovery of the new compound $Sr_{19}Li_{44}$ and refinement of Sr_3Li_2. The existence of two previously reported phases Sr_8Li and Sr_7Li has not been confirmed. The crystal structure of $Sr_{19}Li_{44}$ was

dx.doi.org/10.1021/ic5010165 | Inorg. Chem. 2015, 54, 733−739

investigated by single-crystal and powder XRD as well as by TEM. $Sr_{19}Li_{44}$ can be described as a complicated type of chalcopyrite structure and is a next representative containing novel homoatomic Li anti-Mackay clusters. According to DTA and Guinier measurements, $Sr_{19}Li_{44}$ undergoes peritectoidal decomposition at 148 °C to Sr_3Li_2 and Sr_6Li_{23}. With the help of TEM measurements, the artifacts of doubled cell lengths are explained and $Sr_{19}Li_{44}$ can be assigned to the $Ba_{19}Li_{44}$ structure type.

■ ASSOCIATED CONTENT

Supporting Information

CIF outputs for $Sr_{19}Li_{44}$ and Sr_3Li_2. This material is available free of charge via the Internet at http://pubs.acs.org.

■ AUTHOR INFORMATION

Corresponding Author

*E-mail: smetana@ameslab.gov.

Notes

The authors declare no competing financial interest.

■ DEDICATION

Dedicated to the memory of Prof. John D. Corbett.

■ REFERENCES

(1) Snyder, G.; Simon, A. *Z. Naturforsch.* **1994**, *49b*, 189−192.
(2) Snyder, G.; Simon, A. *J. Chem. Soc., Dalton Trans.* **1994**, *1994*, 1159−1160.
(3) Miller, G. J.; Nesper, R. *J. Alloys Compd.* **1993**, *197*, 109−121.
(4) Fischer, D.; Jansen, M. *Z. Anorg. Allg. Chem.* **2003**, *629*, 1934−1936.
(5) Wang, F.; King, A.; Kanda, F. *J. Phys. Chem.* **1962**, *66*, 2138−2142.
(6) Wang, F.; King, A.; Kanda, F. *J. Phys. Chem.* **1962**, *66*, 2142−2145.
(7) Wang, F.; Kanda, F.; Miskell, C.; King, A. *Acta Crystallogr.* **1965**, *18*, 24−31.
(8) Smetana, V.; Babizhetskyy, V.; Hoch, C.; Simon, A. *Z. Kristallogr.—New Cryst. Struct.* **2006**, *221*, 434−434.
(9) Smetana, V.; Babizhetskyy, V.; Vajenine, G.; Hoch, C.; Simon, A. *Inorg. Chem.* **2007**, *46*, 5425−5428.
(10) Smetana, V.; Babizhetskyy, V.; Vajenine, G.; Simon, A. *Inorg. Chem.* **2006**, *45*, 10786−10789.
(11) Smetana, V.; Babizhetskyy, V.; Vajenine, G.; Simon, A. *Angew. Chem., Int. Ed.* **2006**, *45*, 6051−6053.
(12) Smetana, V.; Babizhetskyy, V.; Hoch, C.; Simon, A. *J. Solid State Chem.* **2007**, *180*, 3302−3309.
(13) Altomare, A.; Burla, M.; Camalli, M.; Carroccini, B.; Cascarano, G.; Giacovazzo, C.; Guagliardi, A.; Moliterni, A.; Polidori, G.; Rizzi, R. *J. Appl. Crystallogr.* **1999**, *32*, 115−119.
(14) Sheldrick, G. M. *Acta Crystallogr., Sect. A* **2008**, *64*, 112−122.
(15) Farrugia, L. *J. Appl. Crystallogr.* **2012**, *45*, 849−854.
(16) Jeitschko, P.; Simon, A.; Ramlau, R.; Mattausch, H. *Eur. Microsc. Microanal.* **1997**, *46*, 21.
(17) Jeitschko, P.; Simon, A.; Ramlau, R.; Mattausch, H. *Z. Anorg. Allg. Chem.* **1997**, *623*, 1447−1454.
(18) Vincent, R.; Midgley, P. A. *Ultramicroscopy* **1994**, *53*, 271−282.
(19) Gjonnes, J.; Hansen, V.; Krerneland, A. *Microsc. Microanal.* **2004**, *10*, 16−20.
(20) Weirich, T.; Portillo, J.; Cox, G.; Hibst, H.; Nicolopoulos, S. *Ultramicroscopy* **2006**, *106*, 164−175.
(21) Gemmi, M.; Zou, X.; Hovmoller, S.; Migliori, A.; Vennstrom, M.; Andersson, Y. *Acta Crystallogr., Sect. A* **2003**, *59*, 117−126.
(22) Own, C. Ph.D. Thesis, Northwestern University, Evanston, IL, 2005.
(23) Goodman, P.; Moodie, A. *Acta Crystallogr., Sect. A* **1974**, *30*, 280−290.
(24) Cowley, J.; Moodie, A. *Acta Crystallogr.* **1957**, *10*, 609−619.
(25) Stadelmann, P. *Ultramicroscopy* **1987**, *21*, 131−146.
(26) *Emaps 1.0*; AnaliteX: Stockholm, Sweden, 2002−2007.
(27) Wilson, C. G.; Spooner, F. J. *Acta Crystallogr.* **1960**, *13*, 358−359.
(28) Tillard-Charbonnel, M.; Belin, C.; Soubeyroux, J. L. *Eur. J. Solid State Inorg. Chem.* **1990**, *27*, 759−769.
(29) Li, B.; Corbett, J. D. *J. Am. Chem. Soc.* **2005**, *127*, 926−932.
(30) Brese, N. E.; O'Keeffe, M. *J. Solid State Chem.* **1990**, *87*, 134−140.
(31) Bärnighausen, H. *MATCH* **1980**, *9*, 139−175.
(32) Kienle, L.; Duppel, V.; Simon, A.; Deiseroth, H. J. *Z. Anorg. Allg. Chem.* **2003**, *629*, 1412−1420.